Biosensors and Bioelectronics ▮ (▮▮▮▮) ▮▮▮–▮▮▮

Contents lists available at SciVerse ScienceDirect

Biosensors and Bioelectronics

journal homepage: www.elsevier.com/locate/bios

Femtogram-level detection of *Clostridium botulinum* neurotoxin type A by sandwich immunoassay using nanoporous substrate and ultra-bright fluorescent suprananoparticles

Sangho Bok [a], Venumadhav Korampally [b], Charles M. Darr [c], William R. Folk [d], Luis Polo-Parada [e,*], Keshab Gangopadhyay [a,f,g], Shubhra Gangopadhyay [g,**]

[a] *Nanos Technologies, LLC Columbia, MO 65203, USA*
[b] *Department of Electrical Engineering, Northern Illinois University, DeKalb, IL 60115, USA*
[c] *Department of Biological Engineering, University of Missouri, Columbia, MO 65211, USA*
[d] *Department of Biochemistry, University of Missouri, Columbia, MO 65211, USA*
[e] *Department of Medical Pharmacology and Physiology, University of Missouri, Columbia, MO 65211, USA*
[f] *Nuclear Science and Engineering Institute, University of Missouri, Columbia, MO 65211, USA*
[g] *Department of Electrical Engineering, University of Missouri, Columbia, MO 65211, USA*

ARTICLE INFO

Article history:
Received 27 June 2012
Received in revised form
25 August 2012
Accepted 31 August 2012

Keywords:
Botulinum toxin
Biosensor
Dye-doped nanoparticle
Immunoassay
Fluorescence

ABSTRACT

We report a simple, robust fluorescence biosensor for the ultra-sensitive detection of *Clostridium botulinum* Neurotoxin Type A (BoNT/A) in complex, real-world media. High intrinsic signal amplification was achieved through the combined use of ultra-bright, photostable dye-doped nanoparticle (DOSNP) tags and high surface area nanoporous organosilicate (NPO) thin films. DOSNP with 22 nm diameter were synthesized with more than 200 times equivalent free dye fluorescence and conjugated to antibodies with average degree of substitution of 90 dyes per antibody, representing an order of magnitude increase compared with conventional dye-labeled antibodies. The NPO films were engineered to form constructive interference at the surface where fluorophores were located. In addition, DOSNP-labeled antibodies with NPO films increased surface roughness causing diffuse scattering resulting in 24% more scattering intensity than dye-labeled antibody with NPO films. These substrates were used for immobilization of capture antibodies against BoNT/A, which was further quantified by DOSNP-labeled signal antibodies. The combination of optical effects enhanced the fluorescence and, therefore, the signal-to-noise ratio significantly. BoNT/A was detected in PBS buffer down to 21.3 fg mL^{-1} in 4 h. The assay was then extended to several complex media and the four-hour detection limit was found to be 145.8 fg mL^{-1} in orange juice and 164.2 fg mL^{-1} in tap water, respectively, demonstrating at least two orders of magnitude improvement comparing to the reported detection limit of other enzyme-linked immunosorbent assays (ELISA). This assay, therefore, demonstrates a novel method for rapid, ultra-low level detection of not only BoNT/A, but other analytes as well.

1. Introduction

The importance of highly sensitive, target-specific sensors has grown dramatically over recent years due to the burgeoning need for diagnostics for chemical and biological toxicants in health care, national security, and food safety industries (Frisk et al., 2011; Yang and Swager, 1998; Fan et al., 2008). Among the various toxins and chemical contaminants known, Botulinum Neurotoxins (BoNT)s are widely considered to be the most potent (Frisk et al., 2011; Bagramyan et al., 2008). The potential use of BoNT in bioweapons is of great concern as reflected in its estimated human lethal dose (LD) of only 1–2 ng kg^{-1} body weight and limitations in medical infrastructure rendering treatment of a widespread outbreak untenable (Arnon et al., 2001; Garcia-Rodriguez et al., 2007; Gill, 1982; Bagramyan et al., 2008). Hence, the detection of low, but nonetheless potent, amounts of BoNT in complex clinical specimens and food represents an extreme, but necessary analytical challenge. Although many Enzyme-Linked Immunosorbent Assay (ELISA) and other kits have been produced in an effort to realize sensitive, specific detection, mouse assays are still considered as the gold standard.

* Corresponding author. Tel.: +1 573 884 4599; fax: +1 573 884 4232.
** Corresponding author. Tel.: +1 573 882 9266; fax: +1 573 884 0312.
E-mail addresses: poloparadal@missouri.edu (L. Polo-Parada), gangopadhyays@missouri.edu (S. Gangopadhyay).

0956-5663/$ - see front matter © 2012 Elsevier B.V. All rights reserved.
http://dx.doi.org/10.1016/j.bios.2012.08.063

Mouse assays, however, are painfully slow (a typical assay taking a minimum of 48–72 h for confirmation) and involve injection of the potential toxin-containing sample into living mice followed by observation for signs of botulinic paralysis or death (Frisk et al., 2011; Bagramyan et al., 2008). Because of this, research on ELISA and other assays for BoNT is still booming as the assays are accurate (typical credential level: 95% or higher), sensitive (detection limit: 9–60 pg mL^{-1}), and an order of magnitude faster than the mouse assay (assay time: 4–8 h) (Bagramyan et al., 2008; Petr Čapek and Dickerson, 2010). Since the LD of BoNT is 1–2 ng kg^{-1}, most available immunoassay detection methods are well-suited as BoNT sensors in terms of detection limit. Nevertheless, there is still room for improvement, especially with regard to response time as a time to detection of less than 1 h is desired while current methods require 4 h at a minimum (Petr Čapek and Dickerson, 2010). Therefore, assays that are fast and simple to use, yet maintain high sensitivities are in immediate need of attention and development.

Fluorescence-based sensors are the preferred detection method for low levels of analyte as fluorescence offers higher specificity to target analytes than amperometric sensors, higher sensitivity than basic colorimetric assays, and higher precision at low levels as fluorescence intensity can be correlated with dye concentration, thereby allowing quantitative determination of captured analyte (Arora et al., 2011). Moving fluorescence biosensors to the next level (i.e. point-of-care diagnostics) requires taking advantage of these strengths while minimizing traditional pitfalls such as photostability and signal-to-noise ratio. However, since conventional planar assays often suffer from low signal-to-noise ratio and offer no means of amplifying positive signal, these assays are largely still limited to the laboratory. Developing platforms capable of intrinsic signal amplification and high signal-to-noise ratio could improve both the detection limit and response time considerably by producing a measurable signal in less time than current methods and a higher build-up of signal over time. Amplifying signal at the substrate level has the added benefit of lowering the burden on detection optics, permitting the use of simple, inexpensive hand-held fluorescence detection units to realize field-deployable, point-of-care diagnostics.

One way of increasing detection sensitivity is by providing an ample number of binding sites for biomolecule immobilization, which can be achieved through the use of high surface area substrates. Alternatively, high sensitivity can be achieved through use of highly fluorescent tags such as quantum dots or dye-doped nanoparticles in the place of conventional fluorescent dyes. Combining these two approaches is therefore expected to result in significantly improved sensitivities. Fluorescence can also be enhanced by employing engineered photonic structures. These include surface plasmon resonant structures (Cui et al., 2010; Tam et al., 2007; Yuk et al., 2010), photonic crystal architectures, and Bragg reflectors. It was also shown that significant fluorescence enhancement may be achieved simply by optimal placement of fluorophores above a reflecting surface (Bras et al., 2004; Volle et al., 2003). As much as an order of magnitude enhancement was demonstrated by placing the fluorophores a quarter-wavelength away from the reflector, invoking constructive interference of both the incident (i.e. excitation) and emitted light.

Here, we demonstrate a novel platform with intrinsic fluorescence signal amplification for highly sensitive detection of BoNT serotype A (BoNT/A). This was accomplished through a synergistic combination of (1) dye-doped organosilicate nanoparticles (DOSNPs) and (2) nanoporous organosilicate (NPO) films (Fig. 1) (Bok et al., 2010, 2012; Korampally et al., 2009). Recently, we reported a novel method to synthesize DOSNPs as fluorescent tags incorporating more than 200 dye molecules within a ~20 nm nanoparticle, increasing the fluorescence intensity 'per label' as compared to free dye molecules (Bok et al., 2012). The dyes are entrapped in a cross-linked nanoparticle cage with a highly hydrophobic core, preventing interaction with aqueous solvents and thus increasing both photostability and resistance to chemical degradation, which is desirable for applications requiring operation in harsh environmental conditions such as extreme pH, temperature, and salt content (Cho et al., 2010; Kim et al., 1999; Zhao et al., 2004). DOSNPs were conjugated to antibodies and found to have an average degree of substitution of 90 dye molecules per antibody (e.g. one DOSNP to two antibodies). NPO films are nanoparticulate organosilicate films characterized by their high surface areas, tunable porosities, and good optical transparency, ideal attributes for a biosensor substrate. (Korampally et al., 2009; Memisevic et al., 2009). These films were engineered to produce constructive interference at the surface where DOSNP-tagged antibodies are captured to maximize collection efficiency. Here, we demonstrate the practicality of these platforms by integrating them

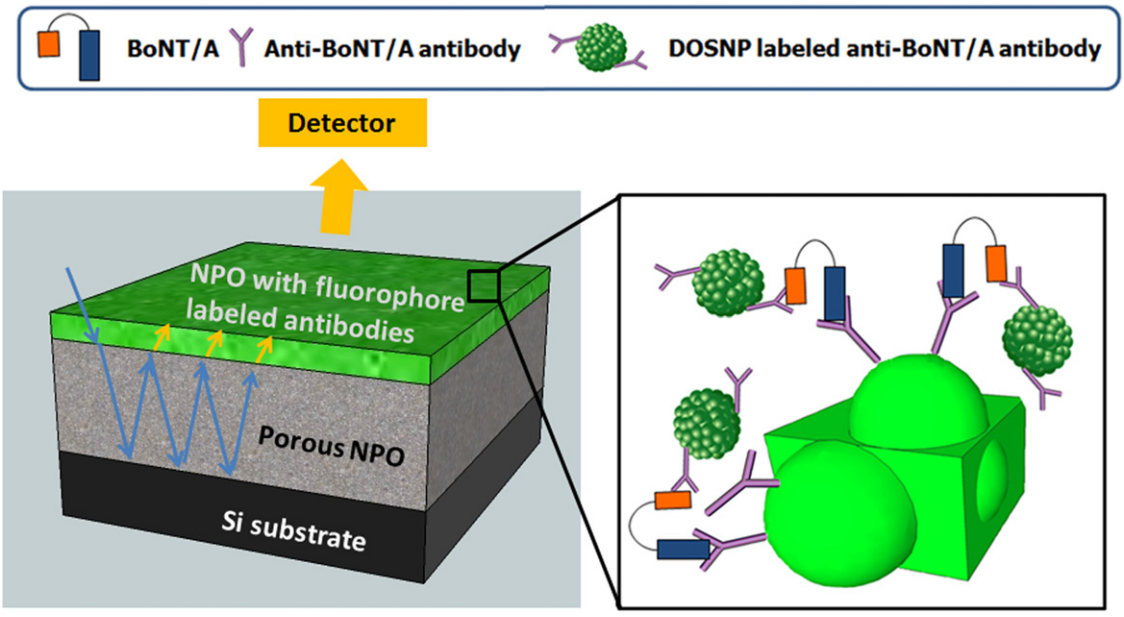

Fig. 1. Schematic of the BoNT/A detection platform with zoomed-in image showing the sandwich assay on the rough surface of NPO substrates.

Please cite this article as: Bok, S., et al., Biosensors and Bioelectronics (2012), http://dx.doi.org/10.1016/j.bios.2012.08.063

with standard 96-well plates. The toxins were detected from spiked tap water and orange juice samples, which are considered to be potential targets of intentional toxin contamination (Wein and Liu, 2005).

2. Materials and methods

2.1. Materials and reagents

Glass resin (GR650F) consisting of flakes of poly (methylsilsesquioxane) (PMSSQ) was purchased from Techneglas, Inc. (Perrysburg, OH) and Rhodamine 6G (Rh6G) from Exciton (Dayton, OH) and used as-is for the preparation of DOSNPs and NPO films. Low-doped p-type silicon wafers were obtained from MEMC, Inc. (St. Louis, MO). 5-(and-6)-Carboxyrhodamine 6G-hydrochloride (CR6G) was purchased from Anaspec, Inc. and used without further modification. Polypropylene glycol (PPG, average molecular weight 425), propylene glycol methyl ether acetate (PGMEA, 98%), 2-[morpholino]ethanesulfonic acid (MES), and phosphate buffered saline (PBS, 10 × concentrate) were purchased from Sigma-Aldrich (St. Louis, MO). EDC (1-Ethyl-3-[3-dimethylaminopropyl]carbodiimide hydrochloride), Sulfo-NHS (N-hydroxysulfosuccinimide), and hydroxylamine hydrochloride (HA-HCl) were purchased from Pierce Biotechnology and used for coupling DOSNP to antibodies and the immobilization of antibodies to NPO films. Monoclonal anti-botulinum antibodies were purchased from [MyBioSource, MBS310475 and MBS310408] and used as received for conjugation. Botulinum neurotoxin type A was purchased from List Biological Laboratories, Inc. and used after reconstitution in PBS. Tap water was collected from a sink in the laboratory, and orange juice was purchased without modification from Simply Orange Company.

2.2. NPO film preparation

The principle of formation of the NPO films and the detailed NPO film preparation has been previously reported (Korampally et al., 2009). Briefly, the wt% composition of the NPO solution for this application was 15:35:50 PMSSQ:PPG:PGMEA, which was deposited onto hydrogen-passivated, low-doped p-type silicon substrates unless otherwise mentioned. Hydrogen passivation was achieved by dipping the silicon substrates in a 1:10 HF:H_2O solution for 30 s immediately prior to film deposition. Films were deposited by dispensing a few drops (~200 μL) of solution on 2 × 2 in. silicon substrate and spin coating at 3000 rpm for 30 s. Following spin coating, the obtained films were immediately subjected to a high temperature calcination step to decompose PPG and induce pore formation by placing the substrates on a pre-heated hot plate (450 °C) for 5 min, after which they were removed and allowed to cool to room temperature.

2.3. Synthesis of the DOSNPs

DOSNPs were prepared according to the method reported previously (Bok et al., 2012). In brief, PMSSQ and Rh6G (mass ratio ~62) were dissolved together in ethanol. Typically, a total of 10 g were prepared in a 20 mL glass vial in a final wt% composition of 1:1:2 PMSSQ:PPG:Ethanol and aged for 3 days in the dark at room temperature. Films were spin-cast on hydrogen-passivated, low-doped p-type silicon substrates and immediately calcined at 250 °C for 35 s, removed, and allowed to cool. The as-prepared film was then treated with CO_2 plasma as described below. Particle suspensions were then made from the nanoparticle films by soaking in deionized water (DIH_2O) for 5 min, rinsing with excess water to remove any free Rh6G, and scraping the film from the substrate using a scalpel blade. The nanoparticulate flakes were dispersed in a few milliliters of water and sonicated in a low-power ultrasonic bath for 30 min. The final obtained solution was filtered through a 0.2 μm filter into a fresh glass vial and stored at room temperature until use.

2.4. Plasma surface modification

Surface modification of DOSNP and NPO films was performed by plasma-enhanced chemical vapor deposition (PECVD, MV Systems, Inc., Golden, CO) as described previously (Bok et al., 2012). Briefly, PECVD plasma was ignited using carbon dioxide gas to achieve carboxyl (–COOH) surface functionality on nanoparticles for subsequent bioconjugation. For NPO films, the conditions used for the plasma treatment were: Base pressure, 20 mTorr; Working pressure, 600 mTorr; CO_2 flow rate, 50 sccm; Power, 7 W; and plasma treatment time, 4 min. For the DOSNP films, the following conditions were used: Base pressure, 20 mTorr; Working pressure, 600 mTorr; CO_2 flow rate, 50 sccm; Power, 20 W; and plasma treatment time, 12 min.

2.5. Fourier Transform Infrared (FTIR) spectroscopic measurement

A Nicolet-4700 FTIR spectrometer was utilized for transmission mode spectral measurements of as-prepared films and CO_2 plasma-exposed films on low resistivity p-type silicon substrates.

2.6. Ellipsometric measurement

Optical characterization of the films was performed using variable angle spectroscopic ellipsometry (VASE^{TM}, J.A. Woollam, Inc.) to obtain film thickness and refractive index (n, measured at 630 nm wavelength). Ellipsometric data Ψ and Δ were acquired at two angles of incidence (60° and 70°) over the spectral range 300–1000 nm (NPO) and 300–1300 nm (DOSNP) in steps of 10 nm. Multiple angles and wavelengths were fit simultaneously using the Cauchy model. Characterization of antibody-immobilized NPO films was performed while the substrates were immersed in the buffer solution using a vertical liquid cell adapter (J.A. Woollam, Inc.) with optical windows for measurements at 70°. Ellipsometric data Ψ and Δ were acquired over the spectral range 300–1000 nm in steps of 10 nm followed by fitting the data with the Cauchy model using water as the ambient layer.

2.7. Scattering measurement

Diffuse scattering of incident light due to the presence of the micron scale surface corrugations was characterized through a home-made optical set-up. A green laser light was shone on the substrates at 30° incidence and the scattered light from the substrates was collected at 90° using an epi-fluorescence microscope equipped with a CCD camera. Digital images of the surface were acquired and processed by ImageJ software to quantify the degree of scattering from the surfaces.

2.8. Atomic Force Microscope (AFM) measurement

Atomic force microscopy (AFM, Model 550, Agilent Technologies) was used to characterize the NPO film after calcination. AFM scans were performed in tapping mode with silicon cantilevers (VP40148, VISTA probes, mean tip radius < 10 nm).

2.9. Antibody labeling

Antibodies were coupled to carboxylated DOSNPs using carboxyl-to-amine coupling chemistry (Bok et al., 2012; Staros et al.,1986). To 1 mL activation buffer (0.1 M MES, 0.5 M NaCl, pH 6.0) was added

0.4 mg EDC and 1.1 mg Sulfo-NHS. Three milligrams (3 mg) of DOSNPs were added and incubated for 15 min in the dark at room temperature. To this solution, 1 mg anti-BoNT/A antibody was added. The pH was changed immediately to 8 with 20 μL 3 M aqueous NaOH. The pH-adjusted mixture was incubated for 2 h in the dark at room temperature with gentle agitation. The reaction was quenched by reacting all remaining intermediates with 10 mM HA-HCl. To compare DOSNP with free dye directly, DOSNPs were replaced in the above protocol with 0.3 mg CR6G. The labeled antibodies were then purified by protein affinity column (Nethery et al., 1990). The labeled antibody was added to protein A-coated magnetic beads (Dynabeads® Protein A, Invitrogen, Inc.). The protein A beads were mixed with antibody solution and incubated for 40 min at room temperature followed by washing with citrate-phosphate buffer (pH 5.0). After washing, elution buffer (0.1 M glycine–HCl, pH 2.8) was added to the beads for elution of the antibody and incubated for 2 min at room temperature with gentle agitation. The low-pH condition dissociated the antibodies from the immobilized Protein A, and the IgG was recovered in its purified state in one or several of the collected fractions. The pH of the supernatant (60 μL) containing labeled antibody was immediately neutralized by adding 6 μL of 1 M Tris buffer (pH 9.0).

2.10. Degree of Substitution (DOS)

Fluorophore- and DOSNP-labeled antibodies were characterized in terms of degree of substitution (DOS), which represents the number of dye molecules attached to each single antibody (Brinkley, 1992). Detailed measurements can be found in the previous study (Bok et al., 2012). In short, DOS can be estimated as follows:

$$\mathrm{DOS} = \frac{[\mathrm{Dye}]}{[\mathrm{Antibody}]} \quad (1)$$

where [Dye] and [Antibody] are the molar concentrations of dye and antibodies, respectively, obtained from the optical absorption measurements of the conjugates. Absorption was measured at 521 nm, 525 nm and 280 nm for DOSNP, CR6G and antibody, respectively.

2.11. Antibody immobilization on NPO films

Antibody was immobilized on plasma-exposed NPO substrates using the same carboxyl-to-amine coupling chemistry described above (Staros et al., 1986). Briefly, 1 mL activation buffer (0.1 M MES, 0.5 M NaCl, pH 6.0) was prepared with 0.4 mg EDC and 1.1 mg Sulfo-NHS. NPO substrates were cut into 5 mm × 5 mm pieces and placed in 96-well plates (Fig. S1). An aliquot of 200 μL activation buffer was then placed atop the pieces in each well. After 15 min incubation at room temperature, 1 μg of anti-BoNT/A antibody was added, the pH was changed to 8 with 4 μL 3 M aqueous NaOH followed by 2 h incubation at room temperature with gentle agitation. The reaction was quenched with the addition of 1 M Tris buffer (pH 9.0). NPO substrates were washed three times with phosphate buffered saline (PBS, pH 7.4) containing 0.1% NP-40 (IGEPAL CA-630, Sigma-Aldrich).

2.12. Botulinum neurotoxin type A assay preparation

Botulinum Neurotoxin Type A (BoNT/A) was reconstituted in PBS (pH 7.4) with a final concentration of 10 μg mL^{-1} as a stock solution. For the detection assay, BoNT/A was further diluted in different media such as PBS, orange juice, or tap water. For individual experiments, 200 μL of the final solutions were used in each well of the 96 well plates.

2.13. Tests and characterization

Antibody-immobilized NPO pieces placed in the 96 well plates were incubated with 200 μL of different concentrations of BoNT/A in PBS, orange juice, and tap water. Samples were incubated at room temperature for 15, 30, 60, or 120 min. The samples were then washed three times in PBS buffer (pH 7.4, 0.1% NP-40). DOSNP-labeled anti-BoNT/A antibody was then added to each sample. The samples were incubated at room temperature for 15, 30, 60, or 120 min and washed again as above. A final aliquot of fresh PBS buffer (pH 7.4, 0.1% NP-40) was added to each well and the fluorescence intensity of the samples was measured in a fluorescence microplate reader (Synergy HT, Bio-Tek Inc.) using 530 nm/25 nm excitation and 590 nm/20 nm emission filters. Background fluorescence of the NPO substrate in PBS buffer alone (no antibody) was subtracted from all readings.

3. Results and discussion

3.1. Assay design

Immunoassays such as ELISA are some of the best-characterized assay formats and are supported by a plethora of standardized equipment and supplies such as multi-well plates and microplate readers. In this report, we have attempted to design our platforms to take advantage of this well-developed infrastructure. Our nanostructured immunoassay involves two steps for detection: (1) BoNT/A is captured and enriched on a porous film-based immunoaffinity matrix (antibody-immobilized NPO films); (2) captured BoNT/A is quantified on addition of fluorophore-labeled antibody. Each step is made possible by a pair of monoclonal anti-BoNT/A antibodies, which complete the sandwich. For efficiency and convenience, the platform can be cut into small pieces (5 mm × 5 mm) and placed in 96 well plates as shown in Fig. S1. This allows for multiple concentrations of a single analyte to be interrogated and offers the opportunity for expansion to test for multiple analytes from a single test bed without fear of cross-talk as in microarray.

3.1.1. Characterization of DOSNP and labeled antibodies

To achieve sensitive detection of BoNT/A, we utilized recently developed ultra-bright DOSNPs having equivalent fluorescence of 212 dyes per particle (Bok et al., 2012). Rh6G was chosen for its thermostability and high quantum efficiency (~0.95). These nanoparticles have excellent photostability shown by the fluorescence half-life of 6.1 h under continuous illumination while the free dyes have a half-life of 0.5 h. The surface-carboxylated DOSNPs have an average zeta potential $\zeta = 16.1 \pm 1.0$ mV, resulting in stable aqueous suspension for several months. Anti-BoNT/A antibodies were conjugated to carboxylated DOSNPs with average degree of substitution (DOS) of 90 fluorophores per antibody with as much as 100 dyes per antibody in some cases (Bok et al., 2010, 2012). It should be noted that typical antibody conjugation with conventional free organic dye molecules results in single digit DOS (equivalent fluorescence of 3–8 dyes per antibody) (Brinkley, 1992). Conjugation is usually limited by both the number of amine groups available for conjugation and optical phenomena such as self-quenching by non-radiative energy transfer, which occurs when multiple molecules of the same fluorescent species are co-localized in close proximity (Brinkley, 1992; Hirsch et al., 2002). In this study, DOS of free CR6G-labeled antibody was estimated to be ~3.1 fluorophores per antibody. The significant increase in DOS using DOSNP is due to the encapsulation of hundreds dye molecules per particle. In principle, labeling one DOSNP per antibody would give DOS ~212. However, the actual DOS (~90 per antibody) suggests that one DOSNP is shared by

Please cite this article as: Bok, S., et al., Biosensors and Bioelectronics (2012), http://dx.doi.org/10.1016/j.bios.2012.08.063

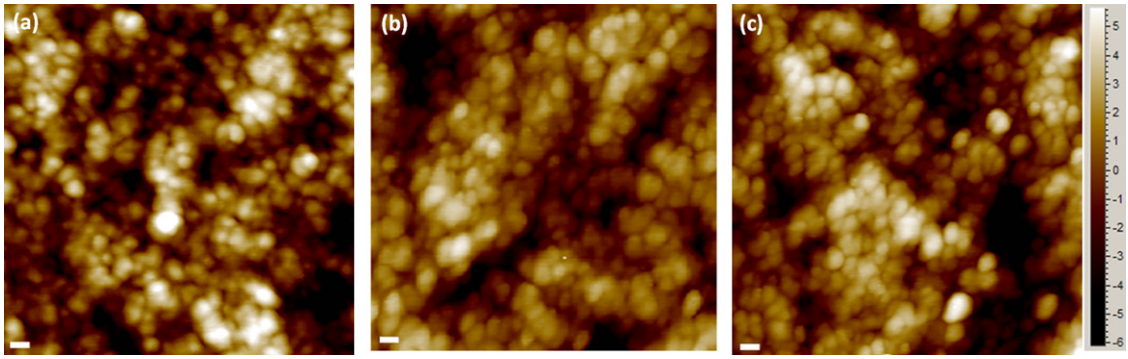

Fig. 2. AFM images of (a) NPO films annealed at 450 °C for 5 min, (b) NPO films with Dylight-549 labeled antibody and (c) NPO films with DOSNP labeled antibody (scale bar: 20 nm).

approximately two antibodies. As the position of the labeling is statistically random, attaching more antibodies per DOSNP may help to ensure that each DOSNP has at least one antibody with an open, available active site.

3.1.2. NPO film characterization

NPO thin films are known to have negligible background fluorescence as compared to plain glass due to the large band-gap of the organosilicate matrix, making them well-suited for use in optical systems such as fluorescence sensors (Bok et al., 2010). This property stems largely from their high porosity as indicated by their refractive index ($n_{avg}=1.098\pm0.02$) [thickness ($t=889\pm19$ nm)] as measured by ellipsometry. Nonporous PMSSQ films typically have a refractive index ~1.38 after cross-linking. Using air ($\varepsilon=1.0006$) as the void fraction, effective medium approximation applying the Bruggeman model suggests a porosity of greater than 70% (Nagy et al., 2006). This is supported by AFM (Fig. 2), which shows a highly porous film with nanoscale surface roughness (mean squared roughness ~4.41 nm). After the sandwich assay, there are no significant changes in size of granules as shown in Fig. 2b and c. This is due to similar scale of antibodies to the granule of the NPO substrates.

The as-prepared NPO films are hydrophobic in nature (water contact angle $>90°$) due to the exposed Si–CH_3 groups on the organosilicate matrix. This is advantageous for the DOSNPs as it prevents aqueous solvents from entering the intraparticle space, but limits the use of as-prepared NPO films for bioconjugation. Surface modification is a critical step for both of these applications. Low-power CO_2 plasma was used to generate surface carboxyl and hydroxyl groups as indicated by the evolution of a C=O asymmetric peak at 1720 cm^{-1} and bonded –OH at 930 cm^{-1} in the FTIR spectrum below (Fig. 3) (Bok et al., 2012). CO_2 plasma exposure time was varied from 2 to 10 min (Fig. S2) and 4 min was chosen as the optimal exposure condition as protein binding was shown to saturate even at longer exposure times and shorter exposures exhibited lower binding efficiency (Fig. S3a). Subsequent antibody immobilization causes an increase in the refractive index at the surface, especially within the top 30 nm of the film as indicated by liquid cell ellipsometric measurement and estimating the antibody refractive index to be 1.45, which is similar to what is reported (Voros, 2004). The as-prepared NPO films have both meso- (2–10 nm), and micro-scale (<2 nm) porosity (Korampally et al., 2009), which limits the antibodies to this upper layer of the NPO films, preventing diffusion of the antibody to the rest of the NPO film. This is beneficial in the end as diffusion rates would limit penetration of any subsequent proteins in the film as well, making only the top layer useful as the binding and detection interface.

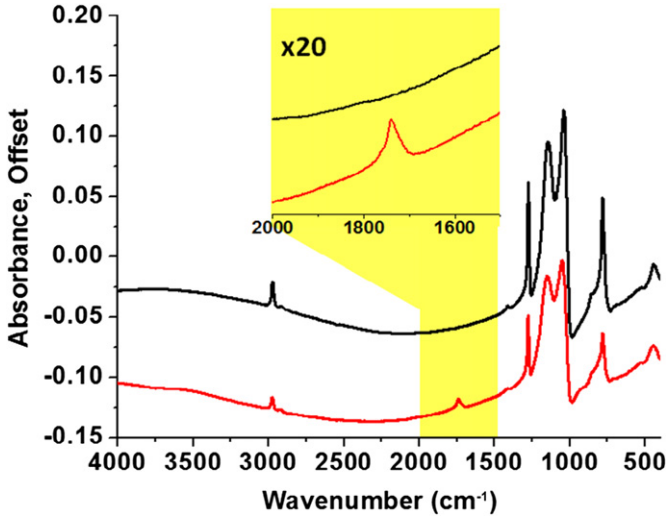

Fig. 3. FTIR spectra of films before (black line) and after 4 min (red line), 7 W CO_2 plasma treatment. Inset is an expanded view showing asymmetric stretching vibration of C=O at 1720 cm^{-1} indicating presence of –COOH groups. (For interpretation of the references to color in this figure legend, the reader is referred to the web version of this article.)

3.1.3. Scattering of NPO films with immobilized antibody

Ellipsometric measurements showed that a dense, high refractive index layer (~1.45) forms at the film-liquid interface when antibodies and analytes are present. This high density layer also produces increased surface roughness leading to more intense light scattering, which can be observed by microscope (Fig. 4). The average scattering intensities were 50, 1154 and 1521 per pixel from silicon, NPO films with dye-labeled antibody and NPO films with DOSNP-labeled antibody, respectively. The highest scattering was observed when NPO films were used in conjunction with DOSNP-labeled antibody rather than dye-labeled antibody while the least scattering from silicon was observed. This scattering behavior is explained by the larger size of DOSNPs than free dye molecules as well as that each DOSNP has two antibodies. The mean surface roughness of the NPO films also increased 15% in assays using DOSNP-labeled antibody compared with assays using dye-labeled antibody (Fig. S4).

3.2. Assay optimization

Using the optimal plasma condition described above, other assay conditions were optimized to maximize sensitivity and minimize detection time for 1 pg mL^{-1} concentration in PBS (Fig. S3b). Analyzing the relative fluorescence with respect to the signal from 4-h incubation time (indicative of typical immunoassay

incubation times) as well as the change in signal gain as a function of assay time, two assay conditions were chosen for comparison with typical immunoassays and other detection methods: 1-h assay time for rapid response and 4-h assay time for highest sensitivity with respect to ELISA and other immunoassays. To reduce nonspecific binding, the assay has been performed in PBS with 0.1% NP-40 as this buffer condition shows similar assay performance to 1% BSA (Fig. S5). Therefore, PBS with 0.1% NP-40 was used for the assay performance.

3.3. Assay performance

Stock BoNT/A was diluted serially in PBS and other complex media and assayed to determine the limit of detection (LOD) in each medium. Each LOD was determined by analyzing the dose–response curves (Fig. 5) to determine the linear response region of the fluorescence signal, indicating a strong correlation between signal and BoNT/A concentration. The linear dose–response was characterized by applying a standard linear regression equation

$$y = a + bx \tag{2}$$

where y is the fluorescence signal x is BoNT/A concentration. The LOD can then be estimated using the following:

$$x_{LOD} = (\eta \times \sigma_{LOD} - a)/b \tag{3}$$

where σ_{LOD} is the standard deviation and η is a confidence factor. The value of $\eta = 1.96$ was chosen for 95% confidence. The fitting parameters for the assay in PBS are summarized in Fig. 5. The LOD in PBS was found to be 21.3 fg mL^{-1} in 4 h total assay time (Fig. 5a). However, rapid response is more practical for real-world samples provided assay performance is sensitive enough to detect a sub-lethal dose (Petr Čapek and Dickerson, 2010). Since the LD of the toxin is in the ng kg^{-1} range and reducing the assay time from 4 h to 1 h leads to only ~20% lower fluorescence intensity,

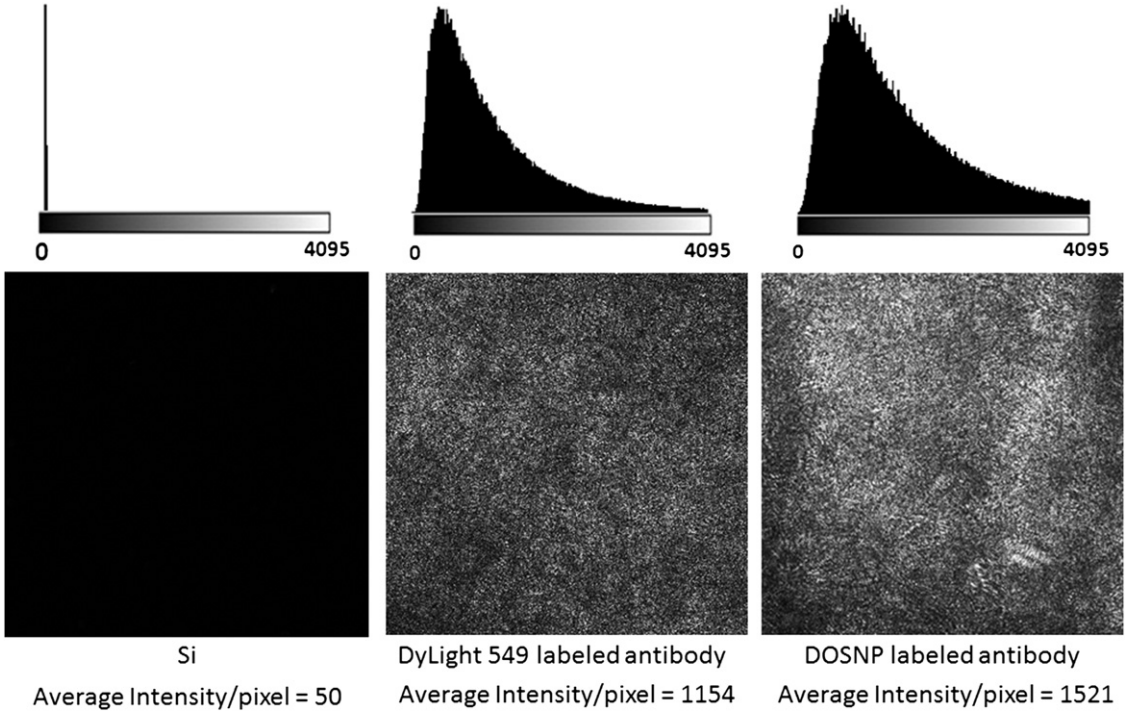

Fig. 4. Scattering intensity from different substrates. A laser (532 nm) was used as incident beam at 30° and the image was captured at 90°.

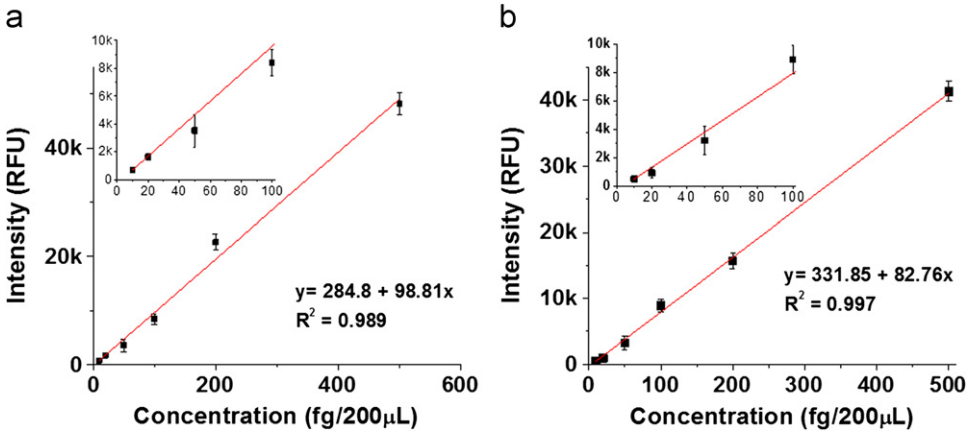

Fig. 5. BoNT/A detection with NPO films and DOSNP-labeled antibodies with assay time: (a) 4 h and (b) 1 h in PBS. Insets are enlarged view of the low concentration region.

Please cite this article as: Bok, S., et al., Biosensors and Bioelectronics (2012), http://dx.doi.org/10.1016/j.bios.2012.08.063

Table 1
LOD comparison of NPO/DOSNP-based platform with different BoNT/A assays.

Methods	LOD (fg mL^{-1})	Assay Time (hours)	Detection Media
Mouse Assay (Kautter and Solomon, 1977)	6×10^3	48	foods, serum, stool
ELISA (Petr Čapek and Dickerson 2010)	$5\times10^3\sim20\times10^6$	4–6	Foods, serum
Immuno-PCR (Chao et al. 2004)	50	4–6	carbonate buffer
ALISSA (Bagramyan et al., 2008)	0.5	2–3	serum, milk, carrot juice
Lateral flow test (Sharma et al. 2005)	$5\times10^6\sim50\times10^6$	0.25	TBS, foods
Our Assay	42.8	1	PBS
	21.3	4	
	382.0	1	Tap water
	164.2	4	
	350.2	1	Orange Juice
	145.8	4	

we do not compromise much in terms of sensitivity while greatly improving real-world applicability (Arnon et al., 2001; Gill, 1982). The 1-h LOD was found to be 42.8 fg mL^{-1} in PBS (Fig. 5b), increasing 2-fold with respect to the 4-h assay. This is due in large part to the increase in error in the shorter assay as well as reduction in signal in the lower concentrations leading to the increase of the intercept values of the linear regression curve.

BoNT/A was also assayed in different complex media (tap water and orange juice) considered to be likely targets of intentional toxin contamination. BoNT/A was still detected in orange juice (145.8 fg mL^{-1}) and tap water (164.2 fg mL^{-1}) at the femtogram level in 4 h. The practical LODs were found to be 350.2 fg mL^{-1} and 382.0 fg mL^{-1}, respectively, for orange juice and tap water in 1 h (Table 1). It should be noted that current ELISA-based detection systems have LODs in the pg mL^{-1} range with at least 4–6 h assay times as summarized in Table 1, meaning that our system is two orders of magnitude more sensitive in PBS and at least an order of magnitude more sensitive in complex media. For comparison with traditional immunoassays, we also performed an assay using CR6G-labeled antibody (DOS ~3.1) with high binding capacity 96-well plates (Fluorolux^{TM} HB, Dynex Technologies, Inc.). Preparation of these assays followed the method reported previously (Goldman et al., 2003). In PBS, the LODs were found to be 51.2 pg mL^{-1} and 20.5 pg mL^{-1} with 1 h and 4 h assay time, respectively (Table S1). Similar tests were performed to estimate the LODs in different complex media and summarized in Table S1. The LODs were found to be in range of 20–300 pg mL^{-1} in 4 h that are higher than the reported limits for typical immunoassays (Table 1) due to the lower DOS of these antibodies.

3.4. Discussion

From an optics standpoint, the sensitivity of a fluorescence based assay relies primarily on the following three factors: the brightness of the fluorescent tags used to tag the detection moieties, their packing density, and the sensitivity of the detection optics. In this paper, we have demonstrated a synergistic approach combining ultra-bright fluorescent nanoparticle probes and high-surface area nanoporous substrates for the sensitive detection of BoNT/A. Nanoporous films are attractive supports for biological assays owing to their large surface areas. Compared to planar surfaces, the three-dimensional porous network offers increased areal density of binding sites for protein/antibody conjugation while ensuring the probes are spaced sufficiently apart to minimize steric effects or autocatalytic degradation of the captured analyte molecules (BoNT/A). The high areal density of the capture probes further enhances the probability of target analyte capture, thereby contributing to the overall sensitivity of the assay.

Despite the large surface areas, the as-prepared NPO films are smooth (with mean-squared roughness value <5 nm) and optically transparent as the nanoparticles and nanoscale voids comprising the film have typical dimensions in the sub-20 nm range. Because the features are much smaller than the wavelength of light necessary to induce any visible Rayleigh scattering, this permits further optimization of these films for fluorescence enhancement through photonic effects. The films in this study were optimized to ensure constructive interference at the surface for both fluorescence excitation and emission. At normal incidence, constructive interference of light due to multiple reflections at the film-air and film-substrate interfaces is maximal at the position of the electromagnetic field anti-nodes located periodically at distances $d_{an}=(2k+1)\lambda/4n$ from the substrate, where k is a positive integer, λ is the wavelength of light in the propagation medium and n is refractive index of the medium (Bras et al., 2004). The thickness of the NPO films were optimized such that the emission fluorescence from Rh6G (548 nm), after multiple reflections at the substrate interface, undergoes constructive interference at the film surface. For constructive interference to occur under these conditions, the required thickness for the film was calculated to be ~848 nm ($k=3$, $n=1.09$) at 528 nm. The thickness of the NPO films was therefore optimized to be in that range. The measured film thicknesses were 889 nm $\pm$ 19 nm, sufficiently close to ensure good fluorescence enhancement at the surface. However, it should be noted that reduced collection efficiencies may occur as a result of using dielectric spacers when multiple reflections cause coupling of the light to the waveguide modes within the dielectric spacer. Therefore, better collection efficiencies may be achieved by introducing micron-scale corrugations/roughness at the dielectric surface, enabling diffuse scattering of light at the dielectric-air interface and consequently preventing total internal reflection at the interface (Liu et al., 2011). Fig. 4 shows a notable increase in the surface roughness of the NPO films on addition of the antibody sandwich, thereby enabling diffuse light scatter and improving the collection efficiency through preventing loss due to waveguiding. Expectedly, sandwich assays employing DOSNP tags exhibited a higher degree of scattering than assays employing fluorophore (Dylight 549) molecules due to the substantially larger size of the DOSNPs (21% higher scattering). It is noteworthy that the large size of the nanoparticles did not hamper the activity of the antibodies during the performance of the assay. This may be understood by examining the degree of substitution of the DOSNP-labeled antibodies. Although the DOSNPs have been characterized to be about 200 times brighter than their constituent single dyes, the calculated DOS value for the DOSNP tagged

antibodies was only 90, suggesting multiple antibodies share a single DOSNP (~2 in this case). This increased the probability of capture of the DOSNP by the target analyte molecules in the sandwich formation.

The relative fluorescence enhancement compared to free dye-labeled antibodies and flat glass substrates by employing various combinations of DOSNPs, conventional fluorescent dyes, NPO films, and glass substrates for sandwich assays for BoNT/A has been shown previously (Bok et al., 2010). Due to the aforementioned synergy, the combined use of the NPO films and DOSNPs gave the maximum enhancement (~540-fold) over the other combinations (Fig. S6).

Table 1 compares the LOD of a BoNT/A assay for different detection schemes. Comparing to published and commercial assays, one of the most sensitive BoNT/A detection systems reported to date is the one by Bagramyan et al., who developed a protease assay with attomolar sensitivity (Bagramyan et al., 2008). However, these assays were based on a two-step approach involving toxin concentration/purification using magnetic beads prior to assaying toxin activity. Compared to the gold standard mouse bioassay as shown in Table 1, the NPO film-based assay was considerably faster and exhibited two orders of magnitude improvement to sensitivity (Chao et al., 2004; Bagramyan et al., 2008; Kautter and Solomon, 1977; Petr Čapek and Dickerson, 2010; Sharma et al., 2005).

4. Conclusions

In conclusion, we have developed a simple, rapid, robust, and sensitive assay for the detection of BoNT/A in simple buffers and complex, real-world samples. Our NPO film-based platform and DOSNP antibody tags ensure both high capture efficiency and femtogram sensitivity, allowing for significant reduction in time-to-detection of sub-lethal doses. Comparison of the limits of detection with both commercial and published assays as well as free dye-labeled antibody and 96-well plates demonstrates superiority of our assay platform by more than 2 orders of magnitude in a typical 4-h assay. Therefore, we propose that the combination of NPO films and DOSNPs provides a viable solution to the long-standing pitfalls of conventional sensing assays (e.g. ELISA, immunofluorescence assays, and the mouse bioassay) such as low sensitivity, long detection times, and photobleaching. Future modification of our assay to encompass other BoNT serotypes, as well as other classes of toxins and contaminants, should be feasible as soon as the necessary substrate reagents become available. Furthermore, the improved sensitivity of these assays reduces the need for complicated optical setups for accurate, sensitive detection and, thus, opens the possibility to develop field-deployable detection systems using handheld fluorescence detection units for point-of-care diagnostics.

Acknowledgments

We gratefully acknowledge financial support from the Leonard Wood Institute (LWI 291-001).

Appendix A. Supporting information

Supplementary data associated with this article can be found in the online version at http://dx.doi.org/10.1016/j.bios.2012.08.063.

References

Arnon, S.S., Schechter, R., Inglesby, T.V., Henderson, D.A., Bartlett, J.G., et al., 2001. Journal of the American Medical Association 285, 1059–1070.
Arora, P., Sindhu, A., Dilbaghi, N., Chaudhury, A., 2011. Biosensors and Bioelectronics 28 (1), 1–12.
Bagramyan, K., Barash, J.R., Arnon, S.S., Kalkum, M., 2008. PLoS ONE 3 (4), 2041.
Bok, S., Korampally, V., Polo-Parada, L., Folk, W.R., Gangopadhyay, K., Dasgupta, P.K., Gangopadhyay, S., 2010. Novel Nanostructured Platform and Nanoparticles for Sensitive Detection of Biological Materials. In: Proceedings of the IEEE Sensors 2010 Conference, pp. 450–453.
Bok, S., Korampally, V., Polo-Parada, L., Mamidi, V., Baker, G.A., Gangopadhyay, K., Folk, W.R., Dasgupta, P.K., Gangopadhyay, S., 2012. Nanotechnology 23 (17), 175601.
Bras, M., Dugas, V., Bessueille, F., Cloarec, J.P., Martin, J.R., Cabrera, M., Chauvet, J.P., Souteyrand, E., Garrigues, M., 2004. Biosensors and Bioelectronics 20, 797–806.
Brinkley, M., 1992. Bioconjugate Chemistry 3, 2–13.
Chao, H.Y., Wang, Y.C., Tang, S.S., Liu, H.W., 2004. Toxicon 43, 27–34.
Cho, E.-B., Volkov, D.O., Sokolov, I., 2010. Small 6 (20), 2314–2319.
Cui, X., Tawa, K., Hori, H., Nishii, J., 2010. Advanced Functional Materials 20 (4), 546–553.
Fan, X., White, I.M., Shopova, S.I., Zhu, H., Suter, J.D., Sun, Y., 2008. Analytica Chimica Acta 620, 8–26.
Frisk, M.L., Lin, G., Johnson, E.A., Beebe, D.J., 2011. Biosensors and Bioelectronics 26, 1929–1935.
Garcia-Rodriguez, C., Levy, R., WArndt, J., Forsyth, C.M., Razai, A., Lou, J., Geren, I., Stevens, R.C., Marks, J.D., 2007. Nature Biotechnology 25, 107–116.
Gill, D., 1982. Microbiology Reviews 46, 86–94.
Goldman, E.R., Cohill, T.J., Charles, H., Patterson, J., Anderson, G.P., Kusterbeck, A.W., Mauro, J.M., 2003. Environmental Science and Technology 37, 4733–4736.
Hirsch, J.D., Eslamizar, L., Filanoski, B.J., Malekzadeh, N., Haugland, R.P., Beechem, J.M., Haugland, R.P., 2002. Analytical Biochemistry 308, 343–357.
Kautter, D.A., Solomon, H.M., 1977. Journal Association Of Analytical Chemistry 60, 541–545.
Kim, H.K., Kang, S.J., Choi, S.K., Min, Y.H., Yoon, C.S., 1999. Chemistry of Materials 11, 779–788.
Korampally, V., Yun, M., Rajagopalan, T., Dasgupta, P.K., Gangopadhyay, K., Gangopadhyay, S., 2009. Nanotechnology 20, 425602.
Liu, R., Ye, Z., Park, J.-M., Cai, M., Chen, Y., Ho, K.-M., Shinar, R., Shinar, J., 2011. Optics Express 19 (S6), A1272–A1280.
Memisevic, J., Korampally, V., Gangopadhyay, S., Grant, S.A., 2009. Sensors and Actuators B: Chemical 141 (1), 227–232.
Nagy, N., Deák, A., Hórvölgyi, Z., Fried, M., Agod, A., Bársony, I., 2006. Langmuir 22 (20), 8416–8423.
Nethery, A., Raison, R.L., Easterbrook-Smith, S.B., 1990. Journal of Immunological Methods 126 (1), 57–60.
Petr, Čapek, Dickerson, T.J., 2010. Toxins 2, 24–53.
Sharma, S.K., Eblen, B.S., Bull, R.L., Burr, D.H., Whiting, R.C., 2005. Applied and Environmental Microbiology 71, 3935–3941.
Staros, J.V., Wright, R.W., Swingle, D.M., 1986. Analytical Biochemistry 156, 220–222.
Tam, F., Goodrich, G.P., Johnson, B.R., Halas, N.J., 2007. Nano Letters 7 (2), 496–501.
Volle, J.-N., Chambon, G., Sayah, A., Reymond, C., Fasel, N., Gijs, M.A.M., 2003. Biosensors and Bioelectronics 19, 457–464.
Voros, J., 2004. Biophysical Journal 87, 553–561.
Wein, L.M., Liu, Y., 2005. Proceedings of the National Academy of Sciences 12, 9984–9989.
Yang, J.S., Swager, T.M., 1998. Journal of the American Chemical Society 120, 11864–11873.
Yuk, J., McDonagh, C., MacCraith, B., 2010. Analytical and Bioanalytical Chemistry, 1–8.
Zhao, X., Bagwe, R.P., Tan, W., 2004. Advanced Materials 16 (2), 173–176.